Plasmonic petal-shaped beam for microscopic phase-sensitive SPR biosensor with ultrahigh sensitivity

Rong Wang,[1,†] Luping Du,[2,†] Chonglei Zhang,[1,†] Zhongsheng Man,[1] Yijia Wang,[3] Shibiao Wei,[1] Changjun Min,[1,5] Siwei Zhu,[3] and X.-C. Yuan[4,*]

[1]*Institute of Modern Optics, Key Laboratory of Optical Information Science & Technology, Ministry of Education of China, Nankai University, Tianjin 300071, China*

[2]*School of Electrical & Electronic Engineering, Nanyang Technological University, Nanyang Avenue, Singapore, 639798*

[3]*Nankai University Affiliated Hospital, Tianjin 300121, China*

[4]*Institute of Micro & Nano Optics, College of Optoelectronic Engineering, Shenzhen University, Shenzhen 518060, China*

[5]*e-mail: cjmin@nankai.edu.cn*

**Corresponding author: xcyuan@szu.edu.cn*

Received September 2, 2013; revised October 2, 2013; accepted October 2, 2013; posted October 3, 2013 (Doc. ID 196621); published November 12, 2013

Differential phase measurement between radially polarized (RP) and azimuthally polarized (AP) beams is an important technique in microscopic surface plasmon resonance (SPR) biosensors as reported in our earlier works [Opt. Lett. **37**, 2091 (2012); Appl. Phys. Lett. **102**, 011114 (2013)]. However, such a technique suffers complex beam splitting, detection, and data processing procedures for RP and AP beams which may lower the accuracy of phase measurement. In this Letter, a novel plasmonic petal-shaped vector beam is proposed instead of RP and AP beams, greatly simplifying the sensor system and enabling single measurement in differential interferometry. Moreover, an improved ultrahigh sensitivity on the order of 10^{-7} refractive index units (RIUs) is experimentally verified in the proposed system.

OCIS codes: (120.3180) Interferometry; (170.3890) Medical optics instrumentation; (180.4243) Near-field microscopy; (240.6680) Surface plasmons; (280.4788) Optical sensing and sensors.

http://dx.doi.org/10.1364/OL.38.004770

Surface plasmon polaritons (SPPs) are electromagnetic surface waves propagating along the interface between dielectric and metal layers due to the collective oscillation of free electrons [1,2]. Owing to the extreme sensitivity of refractive index variations of the dielectric near the interface [3,4], surface plasmon resonance (SPR) effect-based biosensing technique has become a powerful analytical tool over the past two decades in many healthcare applications, such as drug screening, medical diagnostics, immunogenicity, and food safety [5], allowing for real-time and label-free monitoring of the kinetics between macrobiological molecules with high sensitivity.

Among the various SPR biosensing techniques, the phase-sensitive SPR biosensor [6–8] has drawn continuously growing attention due to its extremely high sensitivity. Recently, it is reported that the phase-sensitive SPR biosensor can further be improved by differential phase measurement between transverse-magnetic (TM) and transverse-electromagnetic (TE) polarizations [9,10] in interferometry, utilizing a TM-polarized light to carry SPR phase information and a common-path, TE-polarized light to eliminate the measurement fluctuations. Based on this technique, several new SPR biosensors are proposed using *p*- and *s*-polarized beams in attenuated total reflection configuration [9–11] and using radially polarized (RP) and azimuthally polarized (AP) beams in microscopic configuration in our earlier works [12,13]. However, in these SPR biosensors, multiple synchronized meters required to perform the differential phase measurement increase the difficulties in component alignment and data processing procedures. Moreover, compared to *p* and *s* polarizations split simply by a Wollaston prism, the separation of RP and AP beams requires complex polarization components that induce more deviations. These drawbacks strongly limit the accuracy in SPR phase measurement as well as the maximum sensitivity.

In this Letter, we propose a novel plasmonic petal-shaped vector beam for differential phase measurement in a microscopic SPR biosensor, realizing an exact common-path differential interferometer. Such a beam is sectionalized with alternating RP and AP components in the beam cross section [inset (b) of Fig. 1], which enables measurement with a single beam instead of respective measurements for RP and AP beams, and thus greatly simplifies the excitation, detection, and data processing procedures and increases the accuracy of phase measurement. The petal-shaped SPP field excited by the sectionalized vector beam under tight focusing conditions is investigated both theoretically and experimentally, presenting an excellent agreement with each other. Furthermore, the superior performance of the proposed system is experimentally demonstrated with different concentrations of ethanol solutions.

The diagram of the sectionalized vector beam assisted microscopic SPR biosensor is illustrated in Fig. 1. A He–Ne laser at the wavelength of 633 nm is converted to an AP beam by passing through a spiral phase plate for phase compensating and an azimuthal-type analyzer (AA) for filtering the radial components [14,15]. A half-wave plate is used to convert the generated AP beam into the desired sectionalized vector beam with alternately distributed RP and AP states. We show the polarization vector of AP beam and sectionalized vector beam in insets (a) and (b) of Fig. 1, respectively, where the donut-shaped intensity distribution is owing to the vector

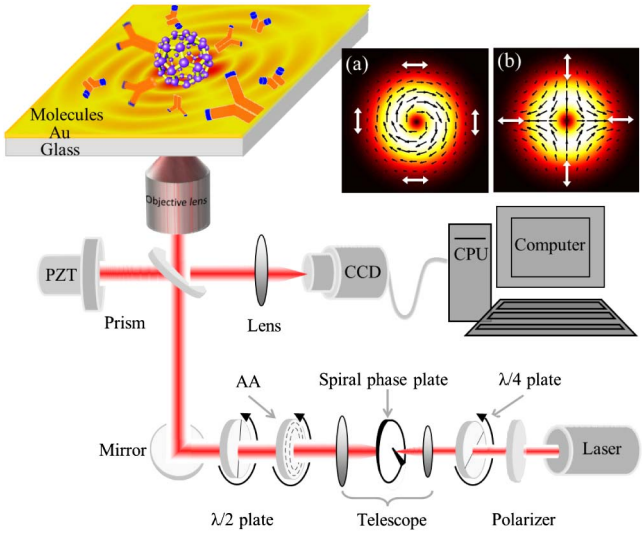

Fig. 1. Experimental setup for microscopic SPR biosensor based on differential phase measurement between radial and azimuthal polarization in a single sectionalized vector beam. Insets show the polarization vectors of (a) an AP beam and (b) a desired sectionalized vector beam with background of intensity distribution. White arrows indicate the polarization direction at different sections in the beam cross section.

singularity at the beam center. Here, we choose the fast axis of the half-wave plate along the diagonal direction, and hence the polarization vectors on both coordinate axes (x and y) of the AP beam are rotated to the radial polarization (indicated by the white arrow), while those on the diagonal directions remain rotated to the azimuthal polarization, as shown in inset (b) of Fig. 1. It is noted that by simply rotating the half-wave plate, the entire beam rotates accordingly without changing the relative polarization state. Such flexibility is important to determining the location of the reference signal when extracting phase information. The generated sectionalized vector beam then illuminates a Michelson interferometer to perform the differential phase measurement. The signal beam is tightly focused onto the glass–gold interface by an oil immersion objective lens (NA = 1.49) to excite SPPs. The thickness of the gold film is 45 nm (±2 nm), well-optimized for phase measurement. For the reference arm, the beam is directly incident onto a silver mirror mounted onto a piezoelectric transducer, introducing a periodic linear phase shift by a triangular wave with an oscillating frequency at 0.02 Hz. In the output path, a 16-bit cooling charge coupled device (CCD) (2048 × 2048, HAMAMATSU, ORCA-Flash4.0) camera is used to detect both the signal and reference signals from their different locations at the beam cross section. Real-time displaying and processing of the interference patterns are performed in a computer connected to the CCD to extract the phase information and calculate the sample's refractive index. Compared to the setup in our earlier work [12,13], only one CCD camera is utilized instead of two synchronized CCDs as the detector and a series of polarization devices for beam splitting are removed simultaneously, hence apparently simplifying the system and reducing measurement error.

The SPP field excited by the proposed sectionalized vector beam under tight focusing conditions is shown in Fig. 2. Due to the fact that RP beam is TM polarized while AP beam is TE polarized when focused, SPPs are excited only at the coordinate axes by the sectionalized vector beam, and then propagate toward the geometric center, resulting in a standing wave pattern after the interference between the counterpropagating SPP waves. Since the polarization direction is same as the radial direction in the x axis but opposite to that in the y axis [as shown in inset (b) of Fig. 1], the excited SPPs in x and y axes under high NA focusing conditions have a phase difference of Π. Therefore, the interference

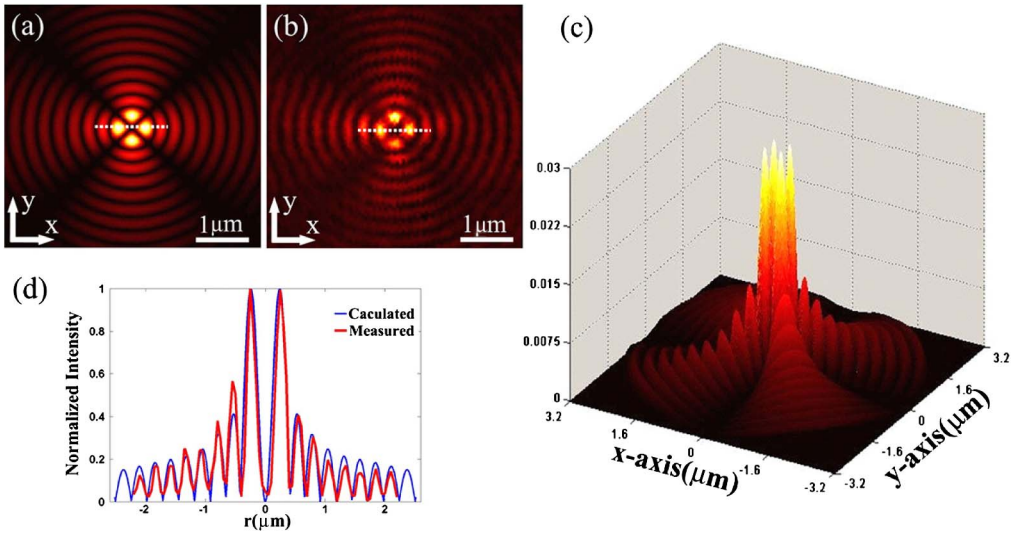

Fig. 2. Theoretically calculated (a) 2D and (c) 3D out-of plane SPP electric field intensity on the gold film excited by the sectionalized vector beam under tight focusing conditions. (b) Experimentally measured SPP electric field intensity distribution by SERS mapping technique. (d) Comparison of normalized measured and calculated profiles of intensity distribution across the white dashed lines in (a) and (b). Both experimental and calculated excitation wavelength is chosen to be 532 nm due to the limited experimental condition.

of SPPs forms a dark center surrounded by four hot spots over a circumference, presenting a petal-shaped field distribution on the gold film. Figures 2(a) and 2(c) show the 2D and 3D plots of the out-of-plane SPP field intensity distribution, respectively, calculated with Richards–Wolf vectorial diffraction method [16,17]. Figure 2(b) gives the experimentally measured SPP field intensity distribution by a new method, referred to as surface-enhanced Raman scattering (SERS) mapping technique [18], which is in excellent agreement with the theoretically predicted one. The comparison of normalized measured and calculated cross-sectional field profiles is plotted in Fig. 2(d), demonstrating the same distribution of peaks. The SPP interference period is measured to be 257 nm, also in good agreement with the calculated SPP half-wavelength of 253 nm.

The CCD camera captures the reflected intensity distributions at the back focal plane of the total internal reflection fluorescence (TIRF) lens, as shown in Figs. 3(a) and 3(b). Due to the coupling of RP components (TM) in a sectionalized vector beam into SPPs, four symmetrically arranged dark arcs are formed at the angular region of the reflected intensity distribution corresponding to the excitation of SPPs, while at the directions where AP components (TE) locate, no SPP is excited because of the polarization mismatch. By rotating the half-wave plate, the dark arcs are also rotated from Figs. 3(a) and 3(b). Figure 3(c), as the sum of Figs. 3(a) and 3(b), shows a complete dark ring at the reflected intensity distribution, in which the position of dark ring indicates the dependence of the resonance angle on the sample's refractive index. The dark ring pattern is then processed with low pass filtering technique and Hough transform to locate the accurate resonance angle [Fig. 3(d)], where differential phase retrieval algorithm is applied to extract the phase shift between the RP and AP components. Such a simple beam superposition procedure helps to accurately locate both the signal and reference data. Moreover, the complex processes of both beam splitting, which involves complicated combination of polarization components, and high-precision image registration between RP and AP images are eliminated. This enables an exact common-path differential phase detection configuration and reduces the deviations induced by optical components and environmental fluctuations. Therefore, the phase shift benefits from the alternating distribution of RP and AP components in a plasmonic petal-shaped beam and can be extracted from one single image instead of two independent ones, greatly improving the measurement accuracy.

To demonstrate the improved performance of the proposed sensing system, ethanol solutions with concentrations ranging from 0.015% to 0.195% with a minor increment of 0.015% are prepared as samples. Three sample fluids with different concentrations are driven simultaneously by the Syringe Pump (BASi, MD-1001) that enables smooth and constant flow at precisely controlled rates ranging from 0.001–500 μL/min with 10 μL – 5.0 mL syringes. The injection of sample fluids into the microchannel is controlled with a Syringe Selector (BASi, MD-1508), capable of quickly toggling one syringe to the next without interrupting flow or introducing air bubbles. Such a controlling system of flows eliminates the pressure change resulting from the short pause of the syringe when changing the solution. Differential phases between the RP and AP components are obtained with a phase retrieve program including shape recognition algorithm, fast Fourier transform, and quadratic fitting. The measured result is shown in Fig. 4, where each data is obtained by averaging differential phases extracted from three continuous measurements. We can observe that the sensor delivers a linear phase shift up to 113.3° within a tiny refractive index range of 1.08×10^{-4} RIU (refractive index unit), indicating an extremely high sensitivity of 9.5×10^{-8} RIU/0.1° within the dynamic range of 0.35 RIU. It is approximately eight times improved compared to our previous results in terms of sensitivity [13]. The detection sensitivity could be further improved with optimized metal film thickness, more stable mechanical structures, better temperature controlling systems, etc.

In this Letter, a novel plasmonic petal-shaped, beam-assisted, phase-sensitive SPR sensing technique was proposed in a microscopic configuration with differential phase measurement between RP and AP components. In the proposed setup, the single measurement mechanism enabled by the plasmonic petal-shaped beam, instead of respective measurements for RP and AP beams, greatly simplifies the experimental setup and the processes of excitation, separation, image registration, and detection, and thus apparently reduces the environmental noise and the errors caused by mechanical vibrations. We verified experimentally the performance of the proposed system and achieved an extremely high

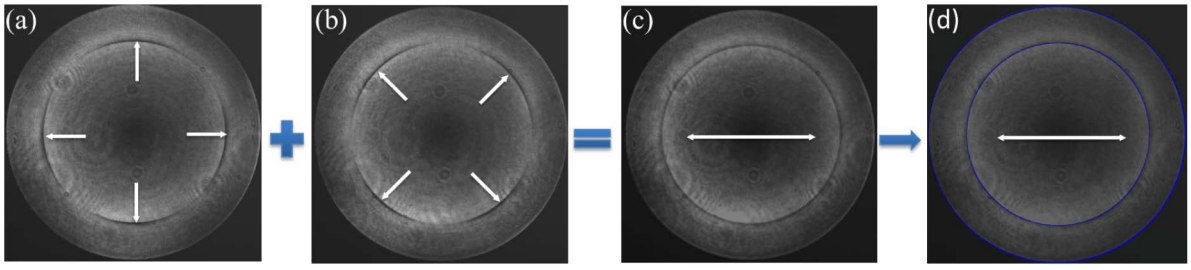

Fig. 3. Intensity distribution of reflection captured by CCD camera at the back focal plane of the objective lens, with the fast axis of the half-wave plate angled (a) ±45° and (b) 0/90° with regard to the horizontal axis. The white arrows indicate the radial polarization directions. The dark arcs correspond to the SPP excitation regions. (c) is the sum of (a) and (b), with a complete dark ring corresponding to the SPR angle. (d) Processed image after digital filtering and a shape recognition algorithm.

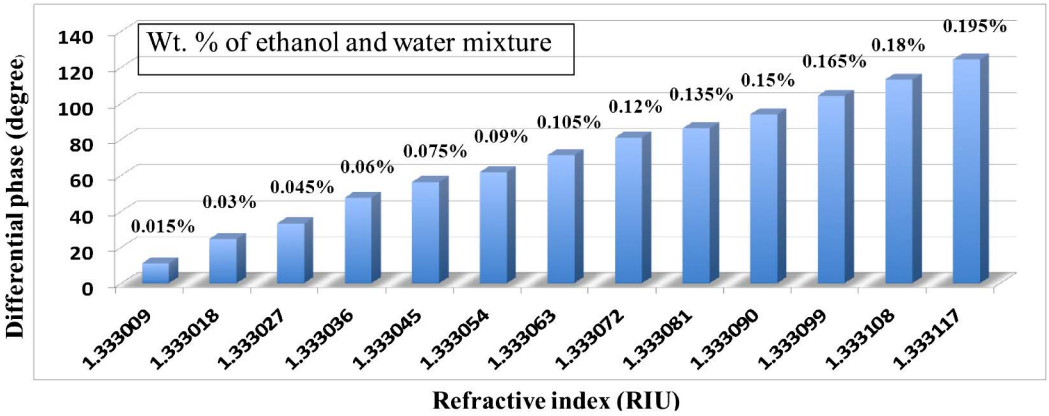

Fig. 4. Differential phase measurement of ethanol solutions with concentration ranging from 0.015% to 0.195%.

sensitivity of 9.5×10^{-8} RIU/0.1°, which is about eight times improvement over our previous result [13]. This system would contribute significantly to the new SPR sensing techniques for determination of biological samples with high sensitivity, large dynamic range, label-free, and real-time capabilities.

This work was partially supported by the National Nature Science Foundation of China under Grant Nos. 61036013, 61138003, and 61377052. X. C. Y. acknowledges the support given by the Tianjin Municipal Science and Technology Commission under Grant No. 11JCZDJC 15200. C. J. M. acknowledges the support provided by the Nature Science Foundation of China under Grant No. 11204141 and Tianjin Municipal Science, and the support provided by the Technology Commission under Grant No. 12JCYBJC31000.

†Authors contributed equally to this Letter.

References

1. A. D. Boardman, ed. *Electromagnetic Surface Modes* (Wiley, 1982).
2. H. Raether, *Surface Plasmons on Smooth and Rough Surfaces and on Gratings*, Vol. **111** of Springer Tracts in Modern Physics (Springer, 1988).
3. J. Homola, S. S. Yee, and G. Gauglitz, Sens. Actuators B **54**, 3 (1999).
4. J. Homola, Anal. Bioanal. Chem. **377**, 528 (2003).
5. R. Karlsson, J. Mol. Recognit. **17**, 151 (2004).
6. S. G. Nelson, K. S. Johnston, and S. S. Yee, Sens. Actuators B **35**, 187 (1996).
7. A. N. Grigorenko, P. I. Nikitin, and A. V. Kabashin, Appl. Phys. Lett. **75**, 3917 (1999).
8. A. G. Notcovich, V. Zhuk, and S. G. Lipson, Appl. Phys. Lett. **76**, 1665 (2000).
9. S. Y. Wu, H. P. Ho, W. C. Law, C. Lin, and S. K. Kong, Opt. Lett. **29**, 2378 (2004).
10. Y. H. Huang, H. P. Ho, S. Y. Wu, S. K. Kong, W. W. Wong, and P. Shum, Opt. Lett. **36**, 4092 (2011).
11. H. P. Ho, W. W. Lam, and S. Y. Wu, Rev. Sci. Instrum. **73**, 3534 (2002).
12. R. Wang, C. L. Zhang, Y. Yang, S. W. Zhu, and X. C. Yuan, Opt. Lett. **37**, 2091 (2012).
13. C. L. Zhang, R. Wang, C. J. Min, S. W. Zhu, and X. C. Yuan, Appl. Phys. Lett. **102**, 011114 (2013).
14. K. J. Moh, X. C. Yuan, J. Bu, R. E. Burge, and B. Z. Gao, Appl. Opt. **46**, 7544 (2007).
15. K. J. Moh, X. C. Yuan, J. Bu, D. K. Y. Low, and R. E. Burge, Appl. Phys. Lett. **89**, 251114 (2006).
16. E. Wolf, Proc. R. Soc. London, Ser. A **253**, 349 (1959).
17. B. Richards and E. Wolf, Proc. R. Soc. London, Ser. A **253**, 358 (1959).
18. L. P. Du, "SPP/LSP coupled hybrid mode directed multi-functional surface-enhanced Raman system," Ph.D. thesis (Nanyang Technological University, 2013).